Analytical Biochemistry xxx (xxxx) xxx

Contents lists available at ScienceDirect

Analytical Biochemistry

journal homepage: www.elsevier.com/locate/yabio

An analytical quality by design approach towards a simple and novel HPLC-UV method for quantification of the antifibrotic peptide N-acetyl-seryl-aspartyl-lysyl-proline

Hei Ming Kenneth Ho [a,b], Satinder Sembi [a], Shorooq Abukhamees [a], Richard M. Day [b], Duncan Q.M. Craig [a,*]

[a] University College London School of Pharmacy, 29-39 Brunswick Square, London, WC1N 1AX, UK
[b] Centre for Precision Healthcare, UCL Division of Medicine, University College London, 5 University Street, WC1E 6JF, UK

ARTICLE INFO

Keywords:
Ac-SDKP
HPLC
Design of experiment
Analytical quality by design
Method development and validation

ABSTRACT

N-acetyl-seryl-aspartyl-lysyl proline (Ac-SDKP) is a tetrapeptide possessing anti-fibrotic, angiogenic, anti-inflammatory, anti-apoptotic, and immunomodulatory properties. Currently, the main method to quantify the peptide is liquid chromatography-tandem mass spectrometry (LC-MS/MS) and enzyme-linked immunosorbent assay (ELISA), both of which are labour intensive and require expensive equipment and consumables. Furthermore, these techniques are generally utilised to detect very low or trace concentrations, such as in biological samples. The use of high concentrations of analyte might overload the extraction column or the separation column in LC-MS/MS or the ELISA plates, so the response could be a non-linear relationship at high analyte concentrations. Thus, they are not ideal for formulation development where detection of dose-equivalent concentrations is typically required. Therefore, a cost-effective, simple, and accurate quantification method for the peptide at a higher concentration needs to be developed. In this study, a simple and novel HPLC-UV method is proposed and validated using an Analytical Quality by Design (AQbD) approach. The method is first screened and optimised using chromatographic responses including capacity factor, resolution, tailing factor, and theoretical plate counts, fulfilling the International Council for Harmonisation (ICH) Q2 (R1) guidelines. The resultant optimised chromatography conditions utilised 10 mM phosphate buffer at pH 2.5 and acetonitrile as mobile phases, starting at 3% (v/v) acetonitrile and 97% (v/v) buffer and increasing to 9.7% (v/v) acetonitrile and 90.3% (v/v) buffer over 15 min at a flow rate of 1 mL/min at the column temperature of 25 °C. The injection volume is set at 10 μL and the VWD detector wavelength is 220 nm. The method established is suitable for detecting the peptide at a relatively high concentration, with a quantifiable range from 7.8 μg/mL to 2.0 mg/mL. In addition, the use of a relatively simple HPLC-UV approach could significantly reduce costs and allow easier access to quantify the peptide concentration. A limitation of this method is lower sensitivity compared with using LC-MS/MS and ELISA methods but running costs are lower and the methodology is simpler. The method is capable to quantify the peptide in various tested matrix solutions, with successful quantitation of the peptide in samples obtained from in vitro drug release study in PBS and from a chitosan-TPP nanogels formulation. Therefore, the method developed here offers a complementary approach to the existing quantification methods, quantifying this peptide at increased concentrations in simple to intermediately complex matrix solutions, such as HBSS, DMEM and FluoroBrite cell culture media.

1. Introduction

N-acetyl-seryl-aspartyl-lysyl proline (Ac-SDKP) is a tetrapeptide cleaved from the N-terminal of thymosin-β4 (Tβ4) via hydrolysis involving meprin-α and prolyl-oligopeptidase, with its structure shown in Fig. 1. It is a naturally occurring immunomodulatory and pro-angiogenic peptide and is degraded by angiotensin-converting enzyme (ACE) into inactive fragments of Ac-SD (N-acetyl-seryl-aspartate) and KP (lysyl-proline). Hence, co-administration of ACE inhibitors, such as captopril, has been suggested to elevate the plasma concentration [1,2].

* Corresponding author.
E-mail address: duncan.craig@ucl.ac.uk (D.Q.M. Craig).

https://doi.org/10.1016/j.ab.2022.114793
Received 31 January 2022; Received in revised form 12 June 2022; Accepted 13 June 2022
Available online 22 June 2022

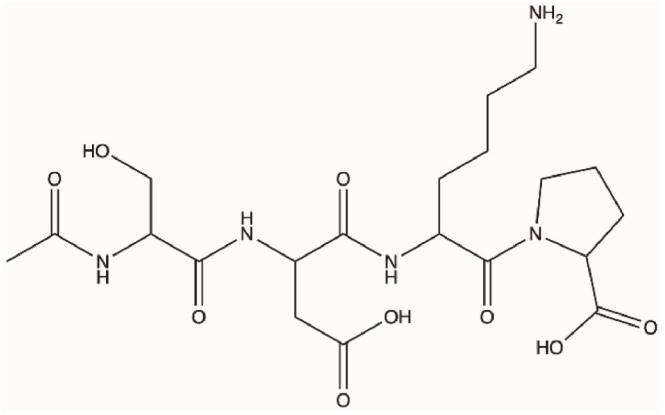

Fig. 1. Structure of N-acetyl-seryl-aspartyl-lysyl proline.

The exact binding site or receptor for Ac-SDKP remains unclear but the peptide is thought to possess angiogenic, anti-fibrotic, anti-inflammatory, anti-proliferative, and anti-apoptotic properties [3]. Consequently, Ac-SDKP has attracted interest in the treatment of renal [4], cardiac [5,6], and lung fibrosis [7], as well as myocardial infarction [8–10].

Given the potential clinical applications of the peptide, a reliable analytical method is required to facilitate the formulation of the peptide, as well as assess the associated in vivo profile. Although a limited number of quantitative assays for the peptide or its analogue have been reported, these techniques either involved enzyme immunoassays (EIA) [11,12] or liquid chromatography-tandem mass spectrometry (LC-MS/MS) [13–16]. Pradelles et al. first described an EIA for Ac-SDKP in 1990, using acetylcholinesterase-Ac-SDKP conjugate as the tracer, rabbit antiserum, and mouse anti-rabbit IgG antibody-coated 96-well plate. However, a limitation of this method was the lack of specificity, resulting in cross-reactivity with Ac-SDKP-like materials [12]. Junot et al. reported an improved EIA assay for the amidated analogue of the peptide, with successful quantification of the peptide analogue in the mouse plasma samples without interference from the endogenous Ac-SDKP. The detection limit in mouse plasma was 1 nM, which is equivalent to 0.5 ng/mL [11]. The same group also published a liquid chromatography-electrospray mass spectrometry (LC-ESI-MS) method for quantifying the Ac-SDKP peptide in human plasma and urine from health volunteers receiving intravenous Ac-SDKP injection or captopril. However, the recovery in plasma was only 64% and the limit of quantitation was 5 ng/mL, as the plasma samples were first extracted using methanol. Detection in urine samples dropped from 88% within the range of 2.5–25 ng/mL to 15% at 1000 ng/mL, indicating an upper detection limit exists using this method for higher concentrations of Ac-SDKP in the samples [16]. Therefore, to overcome these limitations, Inoue et al. reported an LC-ESI-MS/MS method to quantify Ac-SDKP in human plasma samples obtained from the haemodialysis patients, with a wider detection range of 0.5–100 ng/mL and a lower limit of quantitation (LLOQ) of 0.1 ng/mL. Several stable isotope tetrapeptides were used as the internal standard, whilst the samples were extracted via solid-phase extraction before LC-MS/MS [15]. The same group further developed an online solid-phase extraction liquid chromatography-tandem mass spectrometry for high-throughput analysis of the Ac-SDKP peptide in human plasma samples. The LLOQ and range remained unchanged in the new method [13]. Mesmin et al. performed a head-to-head comparison of the LC-MS/MS and EIA method in quantifying the amidated analogue of the peptide in human biological samples and concluded that the LC-MS/MS method offered higher sensitivity and lower assay variability than the EIA [14].

The above methods provide high sensitivity assays for Ac-SDKP but require specialist equipment and non-trivial experimental procedures. Both the LC-MS/MS methods and EIA methods are designed for quantifying Ac-SDKP in biological samples, where the concentration is low and intensive sample preparations are required. The use of high concentrations of analyte might overload the extraction column or the separation column in LC-MS/MS or the EIA plates, so the response could be non-linear, which makes these approaches undesirable to detect analytes with high concentrations. In addition, in vitro drug release is routinely performed in pharmaceutical developments to simulate drug release in the body, where phosphate buffer is commonly used as the medium. However, phosphate buffer is not compatible with the LC-MS/MS, owing to its non-volatile nature. Thus, this study aimed to develop and validate a novel, simple and selective HPLC-UV assay method for the detection of the peptide Ac-SDKP, which is suitable for supporting the development and evaluation of formulations containing the peptide at concentrations commensurate with therapeutic doses, ranging from 400 μg/kg to 3.2 mg/kg per day [6,17]. Moreover, matrix effects of various solutions used in pharmaceutical development were tested, such as HBSS, PBS, chitosan-TPP nanogels, and cell culture media. To the best of our knowledge, no HPLC-UV method was previously reported for the peptide at the time of writing.

The HPLC method was developed using an analytical Quality by Design (AQbD) approach. Quality by design (QbD) is defined by the International Council of Harmonisation (ICH) Q8 (R2) guideline as a systematic approach to development that begins with predefined objectives and emphasizes product and process understanding and process control, based on sound and quality risk management [18]. However, it does not explicitly discuss the requirements for analytical method development. ICH Q9 and Q10 guidelines focus on the risk management and control strategy respectively [19,20], while the ICH Q11 guideline detailed the implementation of QbD in the API synthesis process [21]. While neither of these guidelines is designed for analytical method development, several papers have discussed the implementation of the QbD life cycle in analytical method development, ie. Analytical Quality by Design (AQbD) [18,21–24]. These authors also applied the approach to HPLC method developments according to the ICH Q8 (R2) guideline [25,26]. Aligned with QbD, AQbD applies a similar approach as the typical QbD life cycle, despite the use of different tools and terminology. In brief, the AQbD life cycle includes analytical target profiles (ATP), critical quality attributes, (CQA), risk assessment, method optimisation and development with the design of experiment (DOE), method operable design region (MODR), control strategies, continuous method monitoring and continual improvement [21,27]. The use of AQbD could offer more flexibility for the analytical method, but does require a robust quality system and a deep understanding of the process, product, and analytical method [27]. Therefore, the HPLC method, robustness and ruggedness were tested at the beginning of the method development stage to ensure the efficiency of the method throughout the product life cycle, followed by method validation according to the ICH Q2 (R1) guideline.

2. Materials and method

2.1. Materials

Peptide Ac-SDKP was synthesised by the Chinese Peptide Company (Hangzhou, PRC), with a purity of 90–94%. Acetonitrile (ACN) and hydrochloric acid were purchased from Fisher Scientific (Waltham, MA, USA) while HPLC grade water was obtained from PURELAB® Chorus 2+ machine (ELGA LabWater, High Wycombe, UK). Potassium phosphate monobasic, phosphoric acid and medium molecular weight chitosan were purchased from Sigma Aldrich (St Louis, MO, USA). Sodium triphosphate (TPP) and sodium hydroxide pellet (NaOH) were purchased from Fluka (Switzerland) and VWR (Randor, PA, USA) respectively. Hank's Blank Salt Solution without phenol red (HBSS), penicillin and streptomycin solution (100X), fetal bovine serum, Dulbecco's Modified Eagle Medium (DMEM) with phenol red, and FluoroBrite DMEM were purchased from ThermoFisher (Gibco; Waltham, MA, USA).

Amber HPLC vials caps and cellulose dialysis bag (MWCO 3000) were purchased from Fisher Scientific (Waltham, MA, USA), while the 200 μL conical glass vial insert was purchased from Agilent (Santa Clara, CA, USA). Steritop™ vacuum bottle-top filter and Amicon Ultra filter (MWCO 3000 Da, 0.5 mL) were purchased from Merck Millipore (Darmstadt, Germany). PBS tablet was purchased from MP Biomedicals (Irvine, CA, USA).

2.2. Instrumentation and chromatographic conditions

Chromatographic analysis was performed on an Agilent 1260 Infinity liquid chromatography system (Santa Clara, CA, USA), equipped with a Variable Wavelength Detector (VWD). The column used in the study was a Zorbax Eclipse Plus C18 column (Agilent, Santa Clara, CA, USA), with a particle size of 5 μm, dimensions of 4.6 mm internal diameter and 250 mm in length. The VWD was set at a wavelength of 220 nm and detector sensitivity of 0.1 AUFS. Various flow rates (FR), gradient program, temperature (T), injection volume (V) and pH of the buffer (pH) were used, based on the experimental design matrixes in Tables S1 and S2. 1 mg/mL standard solution of Ac-SDKP in water was prepared and used for the screening and response surface methodology studies.

2.3. Preparation of buffer component of the mobile phase

Phosphate buffer was prepared at a concentration of 10 mM by dissolving 1.36 g potassium phosphate monobasic in 1 L HPLC grade water, with the pH adjusted to 2.5 or 3.0 (±0.05) with the phosphoric acid solution. The buffer was filtered through a 0.22 μm polyethersulfone Steristop™ vacuum bottle-top filter. The buffer was then used immediately upon preparation or stored under refrigeration in borosilicate glass bottles for a maximum period of 24 h.

2.4. Sample preparation

5 drug-free matrices were prepared in this study to explore their matrix effects. Drug-free chitosan-TPP nanogels filtrate (CSNG) was prepared by diafiltration of chitosan-TPP nanogels solution, using the same method as discussed in Section 2.8. Meanwhile, DMEM and FluoroBrite DMEM complete media were first prepared by supplemented respective DMEM with 10% (v/v) heat-inactivated FBS and 1% (v/v) penicillin-streptomycin (100X) solution. Then, the DMEM complete media were diafiltrated using the same method of preparing the nanogels filtrate. Moreover, phosphate buffer saline (PBS) was prepared by dissolving the PBS tablet into HPLC grade water while pre-made cell culture grade HBSS solution was used without dilution. On the other hand, the Ac-SDKP standard solution was prepared by dissolving the Ac-SDKP standard in HPLC grade water at 1 mg/mL. Ac-SDKP samples in other matrix solutions were prepared by mixing the Ac-SDKP stock solution (2 mg/mL) with the respective matrix solution.

2.5. HPLC method development by an AQbD approach

2.5.1. Identification of analytical target profile

The analytical target profile (ATP) sets the criteria to be achieved in the measurement. The proposed method is intended to be an analytical method for estimating the peptides present in pharmaceutical dosage forms (ie. Chitosan-TPP nanogels in this study) and PBS using a reversed-phase HPLC equipped with an autosampler and a quaternary pump. In routine, the method is designed to determine the peptide released in the PBS during the in vitro drug release study and to quantify the unencapsulated peptide in the chitosan-TPP nanogel formulations. Four key outputs in HPLC measurement were identified in the ATP, namely capacity factor (Rf), resolution between the peak of analyte and the closest adjacent peak (Rs), tailing factor for the peak of analyte (Tf), and theoretical plate count (N). The acceptable criteria for these outputs are derived from the ICH Q2 (R1) guidelines, with Rf and Rs ≥ 2, Tf ≤ 1.5 and N ≥ 2000.

2.5.2. Determining critical quality attributes

The critical quality attributes (CQAs) are the method parameters that impact the ATP. Thus, these factors should be controlled to achieve the pre-determined criteria in the ATP. HPLC CQAs usually include mobile phase ratio, pH of the buffer, diluent, column selection, organic modifier, injection volume, flow rate, buffer strength, and elution methodology [21].

2.5.3. Risk assessment, control strategy, continuous method monitoring, and continual improvement

Risk assessments, control strategy, continuous method monitoring, and continual improvement are important parts of the AQbD cycle. These steps were discussed further in the supplementary information.

2.5.4. Definitive screening design

A definitive screening design (DSD) was used for identifying key independent variables impacting the ATP, which was also discussed in the supplementary information.

2.6. Response surface methodology

2.6.1. Experimental design

Response surface methodology (RSM) was used to determine the optimal condition for the chromatographic analysis of Ac-SDKP. A three-level face-centred cubic (FCC) central composite design (CCD) was used in the optimisation, which was formed by five pivotal independent variables as identified from the DSD, namely starting solvent B concentration ($\%B_s$), solvent B concentration increment ($\%B_i$), flow rate (FR), temperature (T) and pH of the buffer. Four key criteria set in the ATP, namely capacity factor, resolution, tailing factor and theoretical plate count (theoretical plate), were determined as the dependent variables. The injection volume (V) and running time were fixed at 20 μL and 15 min to minimise the number of factors in the model, as a run-time of 15 min allows a sufficient time to elute the analyte even at a low percentage of solvent B. The injection volume was fixed at 20 μL to maximise the ranges of detection and quantitation. It is known that any alteration of the injection volume does not hugely affect the capacity factor and theoretical plate number, and thus selectivity and efficiency are maintained. Thus, it is used for fine adjustment on the optimal condition, especially when column overloading happened. Lowering it could further reduce the tailing and improve the resolution. The design matrix to construct the RSM, as shown in Table S2, comprised 21 running conditions and was constructed using JMP 15 software, where each running condition was repeated in triplicate and reported as an average value. Prediction profilers were plotted using the same software. Wash runs were performed in between two different running conditions to equilibrate the column, where a blank solution was run at the set solvent compositions, temperature, and flow rate of the next running condition for 10 min.

A stepwise least squares regression was used to fit the polynomial model to the data individually for each dependent variable. A 5-fold cross-validation was performed to validate the model for all dependent variables. A one-way analysis of variance (ANOVA) test and lack of fit test was conducted to determine the statistical significance and goodness of fit for the model respectively, at a confidence interval (*CI*) of 95%. Response surfaces were plotted to visualise the relationship between independent and dependent variables. A p-value < 0.05 is considered statistically significant. The response surface and contour plots were plotted using the same software.

2.6.2. Multiple response optimisation

Multiple response optimisation (MRO) was used to identify the optimal chromatographic condition for assaying Ac-SDKP, as these

Table 1
HPLC gradient program.

Time (min)	Composition	
	% Solvent A - Phosphate buffer (v/v)	% Solvent B – ACN (v/v)
0	97	3
15	90.3	9.7

dependent variables might contradict each other. The desirability function approach, advocated by Harrington [28], Derringer and Suich [29], transformed the response variables (y_a) into an individual desirability function $d_a(y_a)$, where a number was assigned between 0 and 1. $d_a(y_a) = 0$ indicates a completely undesirable response and vice versa for $d_a(y_a) = 1$. Individual desirability functions were transformed using JMP 15 software (SAS Institute, Cary, NC, USA), to minimise the tailing factor while maximizing the resolution, capacity factor and theoretical plates. Individual desirability functions were then combined into overall desirability, as shown in equation (1).

$$D = \sqrt[a]{(d_1(y_1) \times d_2(y_2) \times \ldots \times d_a(y_a)} \quad (1)$$

where $d_1(y_1)$ *and* $d_2(y_2)$ denote the individual desirability function for factors 1 and 2 respectively. a is the total number of factors while $d_a(y_a)$ is the individual desirability function of factor.

The running condition with the highest overall desirability was considered the optimal condition as determined by JMP 15 (SAS Institute, Cary, NC, USA). The peptide was analysed under the optimal chromatographic conditions in triplicate, with the dependent variables measured experimentally and compared with the predicted values to validate the models.

2.6.3. Optimal running condition

The optimal condition for quantifying the peptide Ac-SDKP was performed with an Agilent Zorbax Eclipse Plus reverse phase C-18 column with a dimension of 4.6 × 250 mm, 5 μm particle size (Santa Clara, CA, USA) to verify the model, at the column temperature of 25 °C. The peptide was eluted using a gradient method as shown in Table 1, at a flow rate of 1 mL/min with 10 mM phosphate buffer at pH 2.5 and acetonitrile was used as the mobile phase. Injection volume was originally set at 20 μL in the MRO but was reduced to 10 μL, minimising the mass overloading. A post-time of 5 min at 97% (v/v) solvent A and 3% (v/v) solvent B was used after each run to re-equilibrate the column.

2.7. Method validation

The method was validated according to the ICH Q2 (R1) guidelines [30], utilising a reported template for best practice [31]. System suitability, linearity, accuracy, repeatability, selectivity, and robustness were evaluated during method validation, with the validation methods discussed individually as follows.

2.7.1. Specificity

Specificity is the ability of the method to determine the analyte from other components in the sample matrix [32], which is usually demonstrated by complete separation of the peak of the analyte from other peaks present in the chromatogram of the sample matrix. Therefore, 10 μL of the Ac-SDKP standard in water, PBS, CSNG, HBSS, DMEM, and FluoroBrite complete media were prepared at 1 mg/mL, which were introduced to the system. In addition, the respective drug-free blank matrix solutions were also introduced to evaluate the specificity of the method.

2.7.2. System suitability

System suitability testing was performed with a 1 mg/mL validation standard solution on two different HPLC systems. A total of 6 injections of the sample were injected. The capacity factor, resolution, tailing factor, and theoretical plates were present as the average, whilst relative standard deviations (RSD) for retention time and peak area were determined.

2.7.3. Linearity and range

Calibration standard solutions were prepared at 8 various concentrations ranged from 0.25 mg/mL to 2 mg/mL. A further 6 concentrations were prepared via serial 2-fold dilutions six repeats to prepare concentrations ranging from 3.9 μg/mL to 0.125 mg/mL. Three individually prepared solutions at each concentration were prepared. Linear regression was employed to determine the correlation. The acceptable criteria of the regression coefficient (R^2) are $R^2 \geq 0.999$. The range was determined on the linear region of the calibration curve.

2.7.4. Limit of detection and limit of quantitation

The lower limit of detection (LOD) and lower limit of quantitation (LOQ) was determined from the calibration curve, according to equations (2) and (3).

$$LOD = \frac{3.3\sigma}{S} \quad (2)$$

$$LOQ = \frac{10\sigma}{S} \quad (3)$$

where σ was the standard deviation of the response and S was the slope of the calibration curve.

2.7.5. Accuracy and quantitative matrix effects evaluation

Spiked samples were prepared at 3 concentrations - 0.75, 1.0, 1.5 mg/mL, using both phosphate buffer and matrix solutions. Three individually replicates at each concentration were prepared and analysed. The mean, standard deviation, RSD, and percentage recovery were evaluated, and the acceptance criteria are RSD <10%. Evaluation of the matrix effects was performed by comparison of the slopes of the curves constructed by PBS and placebo, with the slope of the calibration curve in water. A one-way ANOVA was performed on GraphPad Prism 9 to determine if the matrix effect was statistically significant, where a p-value <0.05 is considered statistically significant.

$$Matrix\ effect = \left(\frac{S_{matrix}}{S_{std}} - 1\right) \times 100\% \quad (4)$$

where S_{matrix} was the slope of the curve constructed by PBS and placebo. S_{std} was the slope of the calibration curve in water.

2.7.6. Repeatability and intermediate precision

A 1 mg/mL Ac-SDKP solution in water was prepared and 10 replicates of the validation standard were injected to determine the instrumental precision. The result was reported as average, standard deviation and relative standard deviation (RSD) of the retention time, peak area, and height. The acceptable criteria were within 1% of the RSD for these parameters. Meanwhile, intermediate precision determined the intra-lab variations. Three solutions with concentrations of 0.5, 1.0 and 1.5 mg/mL Ac-SDKP were prepared and performed on two different HPLCs (Agilent 1200, Santa Clara, CA, USA) on two different days by two operators. The relative standard deviation for each operator and each instrument was determined and reported. The acceptable criterion was RSD within 2% [30].

2.7.7. Robustness

The robustness of the method was tested with deliberate alterations in the flow rate, $\%B_s$, temperature, and pH of the mobile phase to determine the capacity of the method to remain unaffected by variations in the method parameters. Variations of flow rate, $\%B_s$, temperature and pH were selected as ±0.2 mL/min, ±1%, ±5 °C and ±0.1 respectively. Thus, buffers with pH of 2.4 and 2.6 were prepared. The robustness of

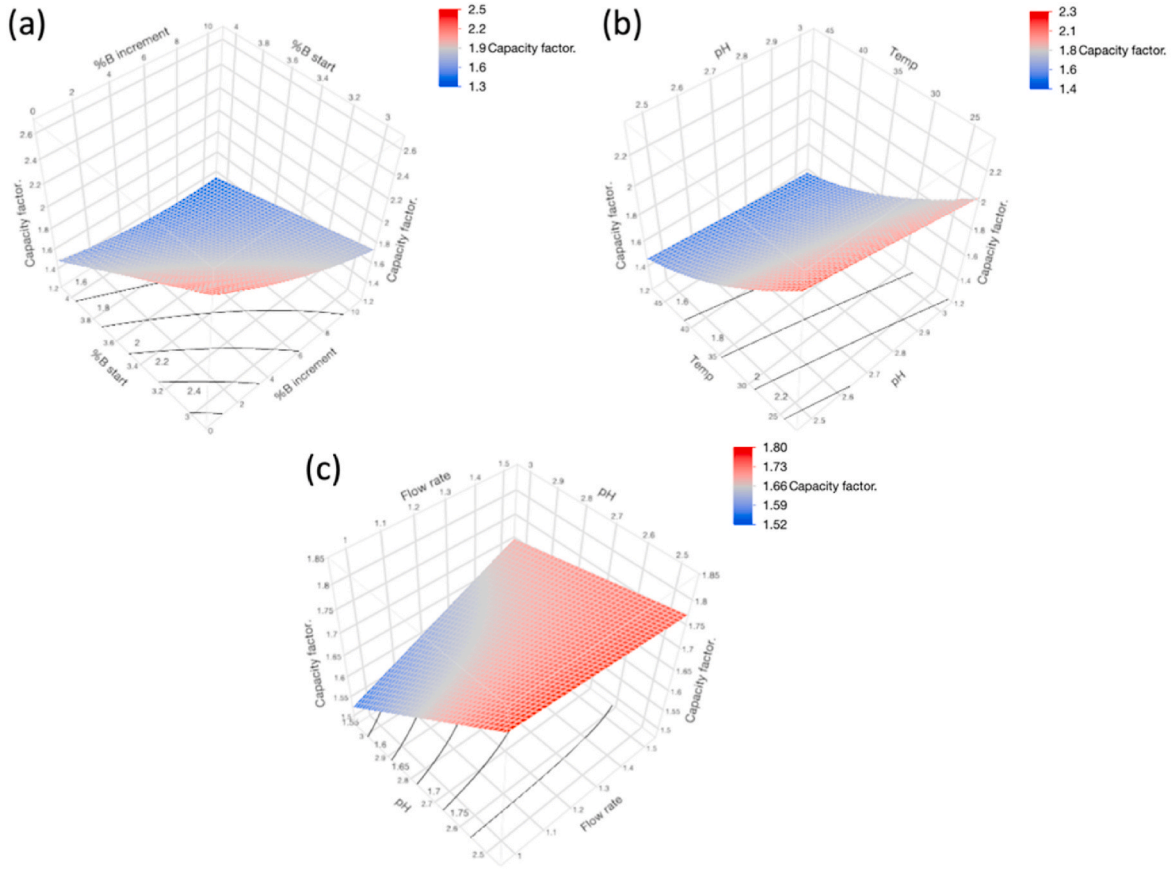

Fig. 2. Response surface models predict the effect of (a) starting % solvent B and %B increment, (b) pH and temperature and (c) flow rate on the capacity factor of the analyte peak.

the method was assessed using two aspects – the peak area and capacity factors of the analyte peak. For capacity factors, the predicted values were calculated from the chromatographic conditions of the deliberate alterations using the correlation established in the MODR. The assays were then performed in triplicate to obtain the experimental result. Percentage differences between the two values were calculated as described in equation (5). Regarding the peak area, it is not an identified ATP, so the percentage difference was calculated using equation (6), between the peak area obtained in the optimal condition and conditions with deliberate alterations.

$$\%\ Difference = \frac{Rf_{experimental} - Rf_{predicted}}{Rf_{predicted}} \times 100\% \quad (5)$$

$$\%\ Difference = \frac{Peak\ Area\ _{Alterations} - Peak\ Area\ _{opt.}}{Peak\ Area\ _{opt.}} \times 100\% \quad (6)$$

where $Rf\ _{predicted}$ and $Rf\ _{experimental}$ refer to the predicted and experimental capacity factor of the analyte peak respectively. $Peak\ Area\ _{Alterations}$ and $Peak\ Area\ _{opt.}$ corresponded to the measured peak area for the analyte peak in the chromatographic conditions with deliberate alterations and the optimal condition respectively.

2.8. Determining the encapsulation efficiency and drug release of Ac-SDKP from chitosan-TPP nanogels

Ac-SDKP loaded chitosan-TPP nanogels were fabricated using the method previously described by our group [33]. In brief, medium molecular weight chitosan was first dissolved in 1% (v/v) hydrochloric acid to produce a 0.1% (v/v) solution. The pH of the solution was adjusted to pH 4.5 with 0.1 M sodium hydroxide solution. Ac-SDKP was then added to the chitosan solution at a concentration of 2 mg/mL 10 mg of TPP was dissolved in 30 mL HPLC grade water to obtain a chitosan-TPP ratio of 3. An equal volume of the TPP solution was finally added to the chitosan solution under stirring at 50 °C. The solution was stirred at 600 rpm for 1 h.

Encapsulation efficiency (EE) of Ac-SDKP in the chitosan-TPP nanogels and preparation of drug-free matrix sample was performed using the same method, with Ac-SDKP-loaded nanogels and drug-free nanogels used respectively. For EE, 0.5 mL of the Ac-SDKP-loaded nanogel solution was added into a 0.5 mL Amicon diafiltration tube (MWCO 3000; Merck Milipore, Billerica, MA, USA). The solutions were then centrifuged using at 14000×*g* for 30 min at 4 °C using a refrigerated mini centrifuge (Heraeus Fresco 17, Thermo Scientific, Waltham, USA), the filtrate was isolated and assayed by this HPLC assay method. EE was calculated using equation (7). The experiment was repeated three times and the results were presented as mean ± SD. For CSNG matrix sample preparation, 0.5 mL of drug-free chitosan-TPP nanogels was added into the Amicon filter, and the filtrate obtained was the matrix sample.

$$EE = \frac{Peptide_{Added} - Peptide_{Free}}{Peptide_{Added}} \times 100\% \quad (7)$$

where $Peptide\ _{Added}$ and $Peptide\ _{Free}$ refer to the amount of peptide added initially and the amount of unencapsulated peptide respectively.

A drug release study was performed in 20 mL PBS (10 mM, pH 7.4) solution with continuous stirring at 37 °C over 24 h 2 mL of the nanogels solutions were loaded into a cellulose dialysis bag (3500 MWCO, volume/cm = 1.91, Fischer Scientific, Waltham, MA, USA) with both ends tied, followed by submerging into PBS. 0.25 mL aliquots were withdrawn at certain time points and an equal volume of fresh preheated PBS solution was added to maintain a constant volume. Ac-SDKP released

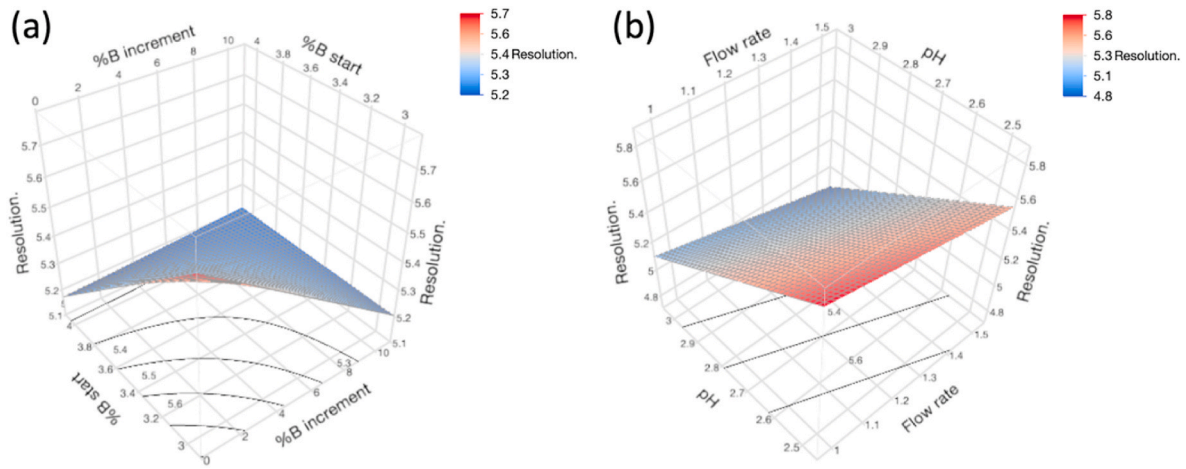

Fig. 3. Response surface models predicting the effect of (a) starting % solvent B and %B increment, (b) pH and flow rate on the resolution.

was assayed by this HPLC method. The experiment was replicated independently three times and the results were presented as the mean value ± standard derivation.

3. Results and discussion

3.1. Central composite design

3.1.1. Statistical analysis

The response surface model for each dependent response, namely capacity factor, resolution, tailing factor, and the number of theoretical plates was constructed with a polynomial equation. A one-way analysis of variance (ANOVA) and lack of fit test was performed on the RSM for each individual dependent variable to determine the statistical significance and the goodness of fit of these models respectively. The null hypothesis of the ANOVA is that these models do not correlate with the data set. The results of the ANOVA and lack of fit tests are reported in Table S3 *p*-values obtained in the ANOVA test for all the models were smaller than 0.05, demonstrating the significance of these models. Terms, with linear effects, interactions, and quadratic effects included in the polynomial equations were also shown in Table S3, with the significance of these terms evaluated individually. Furthermore, the *p*-values in the lack of fit tests for all models were larger than 0.05, which indicated these relationships were a good fit for the data set. Thus, the results showed that the models established in the RSM were correlated strongly with the data set and were well-fitted. The predictive capacity of these models within the design space is maintained.

3.1.2. Method operable design region (MODR)

3.1.2.1. Capacity factor. The capacity factor, aka. the retention factor indicates the retention of the analyte in the column in reference to the dead volume (t_0). All the chromatographic runs in Table S2 possessed capacity factors above 1, which indicated that the retention of the analyte in the column is sufficient, and the specificity of the analyte is achieved under these chromatographic conditions. All factors, except the quadratic term of $\%B_i$ and the interaction term between $\%B_i$ x pH, were statistically significant in the ANOVA test as presented in Table S3. Increasing in all linear terms resulted in a reduction of the capacity factor, as the interactions between the sorbent and analytes were weakened and thus the retention in the column was reduced. In contrast, all the statistically significant interaction terms possessed positive effects on the capacity factor, which indicated that there are synergies between the linear factors and these synergist interactions attenuate the reduction of capacity factors at a high level the linear factors. The quadratic term of the temperature also possessed a positive coefficient, which demonstrated that the effect of temperature was not linear and the effect of temperature on capacity factor was enervated at high temperature as shown in Fig. 2, likely as a result of simultaneous altering of the chemical and mechanical factors in the kinetics of the analyte in the column in elevated column temperature. The results revealed that lowering these parameters could promote the interaction between the peptide and the column and thus increased the capacity factor.

$$\begin{aligned} \textit{Capacity factor}\ (k) = {} & 13.5123 - 0.3975 \times \%B_i - 1.4860 \times \%B_s - 2.3494 \\ & \times FR - 1.5078 \times pH - 0.14864 \times T + 0.002 \times \%B_i^2 + 0.0006 \times T^2 \\ & + 0.0477 \times \%B_s \times \%B_i + 0.03479 \times \%B_i \times FR + 0.0192 \times \%B_i \times pH \\ & + 0.0020 \times \%B_i \times T + 0.2051 \times \%B_s \times FR + 0.0109 \times \%B_s \times T + 0.5673 \\ & \times FR \times pH + 0.0115 \times pH \times T \end{aligned} \tag{8}$$

3.1.2.2. Resolution. Resolution is a measure of the separation between two peaks in a chromatogram in terms of distance and width [34]. In this study, the resolution measured the separation between the peak of interest and the closest adjacent peak using the half-height method. The adjacent peak was at the retention time of 5.7 and 5.955 min as shown in Fig. 7. The measured resolution for all chromatographic runs in the design matrix was above 4, which indicated that the separations between the peak of interest and the adjacent peak were sufficient. The response surface plots for resolution are shown in Fig. 3. $\%B_s$, $\%B_i$, flow rate, and pH were found to have significant but negative effects on the resolution, as the coefficients for these terms were negative in equation (9). Increasing flow rate and steepness of the gradient generally decreased the resolution as both narrowed the peak spacing in the chromatogram [35]. Altering the pH was more complex, as it changed both selectivity and retention, of which both subsequently impact the resolution. However, the response surface plots showed that the overall effect of pH was negative, which indicates that the resolution decreases with the pH of the buffer for this peptide. In contrast, the use of higher organic solvent composition reduced the retention of the peptide as it decreased the polarity of the mobile phase and thus the peak spacing. Meanwhile, the interaction term between $\%B_s$ and $\%B_i$ was also found to be significant, which indicated that there is a synergism between $\%B_s$ and $\%B_i$ in changing the resolution (see Fig. 3).

$$\begin{aligned} \textit{Resolution} = {} & 10.7083 - 0.1638 \times \%B_i - 0.4433 \times \%B_s - 0.4229 \times FR \\ & - 1.1600 \times pH + 0.0408 \times \%B_s \times \%B_i \end{aligned} \tag{9}$$

3.1.2.3. Tailing factor. The tailing factor refers to the coefficient of peak symmetry in United States Pharmacopeia (USP) and the acceptable tailing factor is between 0.9 and 1.2. Only a quarter of the

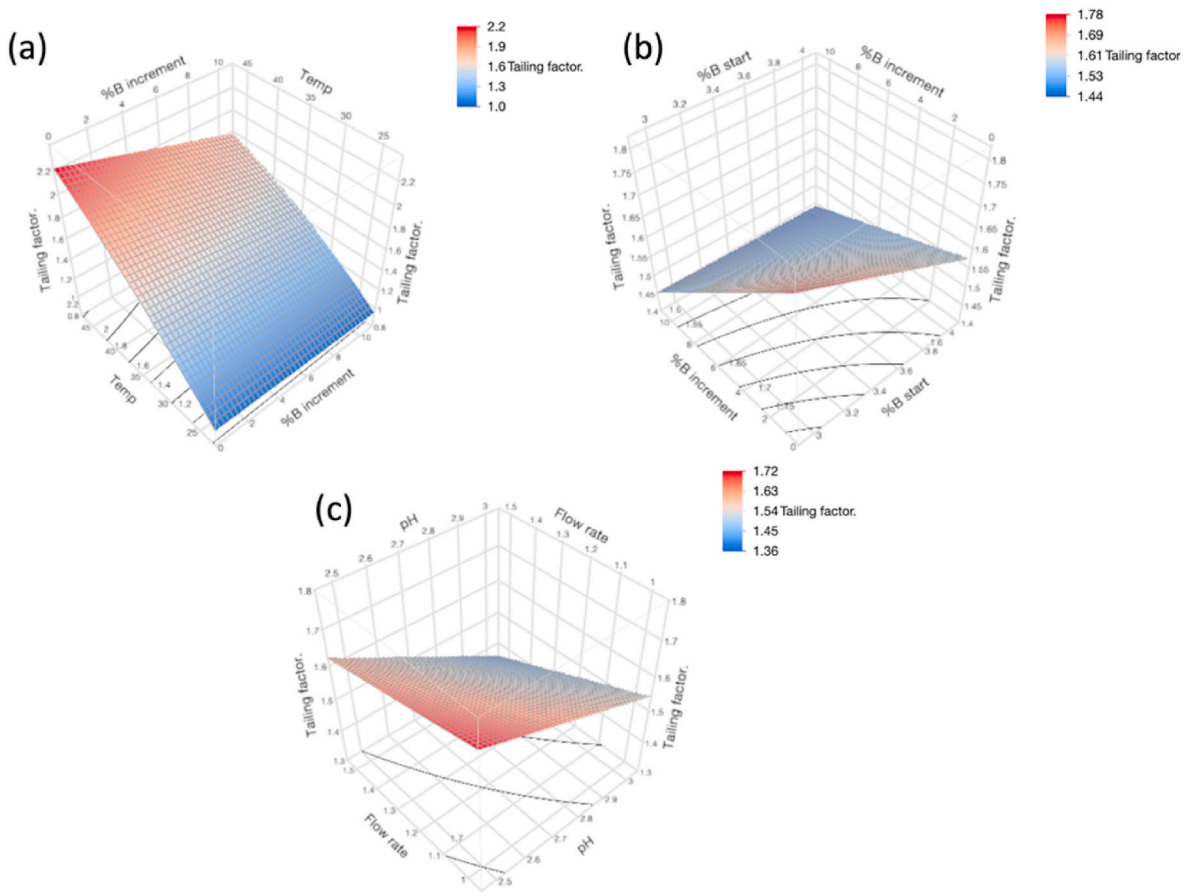

Fig. 4. Response surface models predict the effect of (a) temperature, (b) starting % solvent B and %B increment, and (c) pH and flow rate on the tailing factor of the analyte peak.

chromatographic conditions in Table S2 possessed a tailing factor in between the acceptable criteria. The ANOVA study demonstrated all the linear terms of the factors were significant, with $\%B_i$ and pH reducing the tailing and vice versa for $\%B_s$, FR, and T. Increase in $\%B_i$, specifically the gradient steepness, refocused the peak and minimised the peak tailing. Interestingly, increasing pH reduced the tailing factor as shown in Fig. 4, most likely due to the pH being close to the isoelectric point of the peptide. Increasing the flow rate resulted in higher tailing factors, which is potentially due to increased mass transfer and diffusion of the analytes at a higher flow rate. Elevating the column temperature also led to a higher tailing factor, as the column temperature influences the kinetics and transport properties of the analytes. The diffusivity of the analyte was enhanced because the viscosity of the mobile phase decreased at a higher temperature. Nonetheless, the correlation between flow rate, temperature, and $\%B_s$ with the tailing factor is poorly understood. Several interactions between $\%B_s \times \%B_i$, $\%B_i \times$ pH, $\%B_i \times$ T, $\%B_s \times$ T, and the quadratic term of temperature, were also found to be significant in controlling the tailing factor. However, it is difficult to identify the causes between the interaction terms and tailing factor as peak tailing is occurred due to multiple retention mechanisms of the analyte in the column. The peptide used in this study interacts via nonspecific hydrophobic interactions with the C18 chain and the polar interactions with the ionised residue of the silanol groups. In addition, there are also interactions between the analytes as the peptide remains predominantly cationic at pH 2.5–3.0, where the repulsion between the analyte resulted in mass overloading of the column. Another possible explanation is that peak broadening was a consequence of the cationic peptides repulsing each other in the stationary phase.

$$\begin{aligned} Tailing\ factor = & -0.6694 - 0.0758 \times \%B_i + 0.2281 \times \%B_s + 0.8999 \times FR \\ & - 0.1890 \times pH + 0.1077 \times T - 0.0005 \times T^2 + 0.0144 \times \%B_s \times \%B_i \\ & + 0.0210 \times \%B_i \times pH - 0.0015 \times \%B_i \times T - 0.1379 \times \%B_s \times FR \\ & - 0.0064 \times \%B_s \times T - 0.2391 \times FR \times pH \end{aligned} \quad (10)$$

3.1.2.4. Theoretical plate counts. The number of theoretical plates is an indication of the column efficiency. All factors identified in Table S3 were statistically significant in controlling the number of theoretical plates. The response surface plots for theoretical plate counts are shown in Fig. 5. $\%B_s$, flow rate, temperature, and pH were found to have significant but negative effects on the theoretical plate counts, as the coefficients for these terms were negative in equation (10). Increasing all these factors reduced the column efficiency, as the retention time was reduced and the standard deviation of the measured peak in the unit of time was also altered [36]. Conversely, $\%B_i$ was also significant and possessed a positive effect on the number of theoretical plates. The result demonstrated that steepening the gradient slope within the design space improved the column efficiency, which is likely due to refocusing of the peak with the steeper gradient. Several interaction terms, namely $\%B_i \times \%B_s$, $\%B_i \times$ FR, $\%B_s \times$ T, and $\%B_s \times$ FR, were found statistically significant in the ANOVA, where the former three terms and the last term had negative and positive effects on the theoretical plate counts respectively. Another quadratic term of temperature was also statistically significant, with the peak trough identified at about 35 °C.

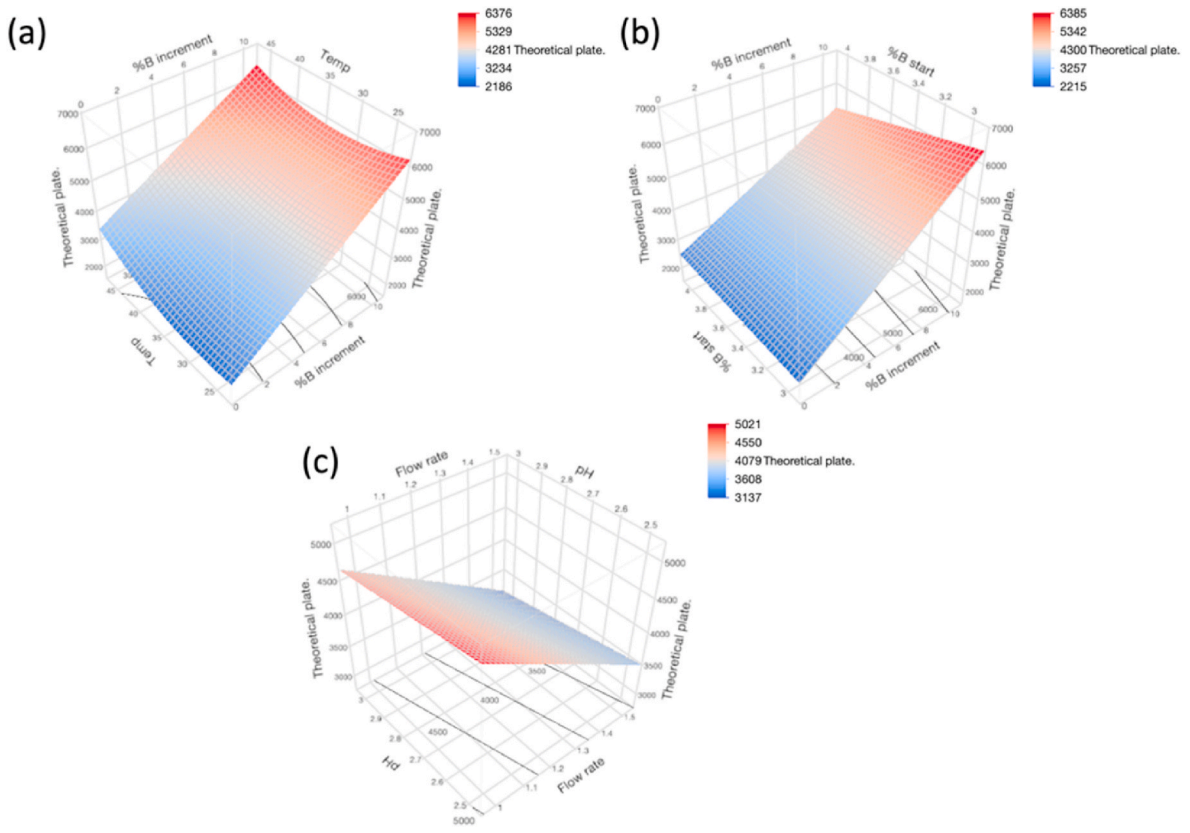

Fig. 5. Response surface models predict the effect of (a) temperature, (b) starting % solvent B and %B increment, and (c) pH and flow rate on the number of theoretical plates.

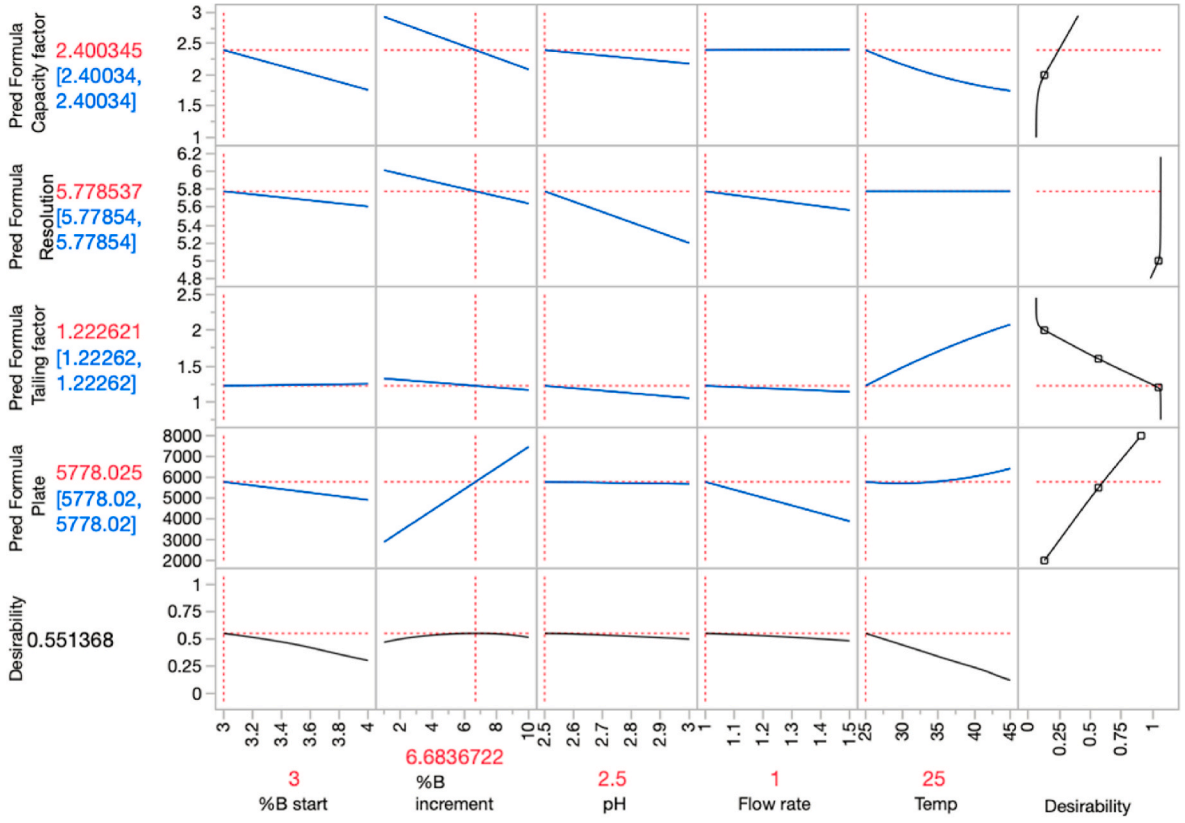

Fig. 6. Interaction profilers show the optimal chromatographic condition with the predicted parameters. %B $_{increment}$ was rounded to 1 decimal place to reflect the sensitivity of the HPLC program.

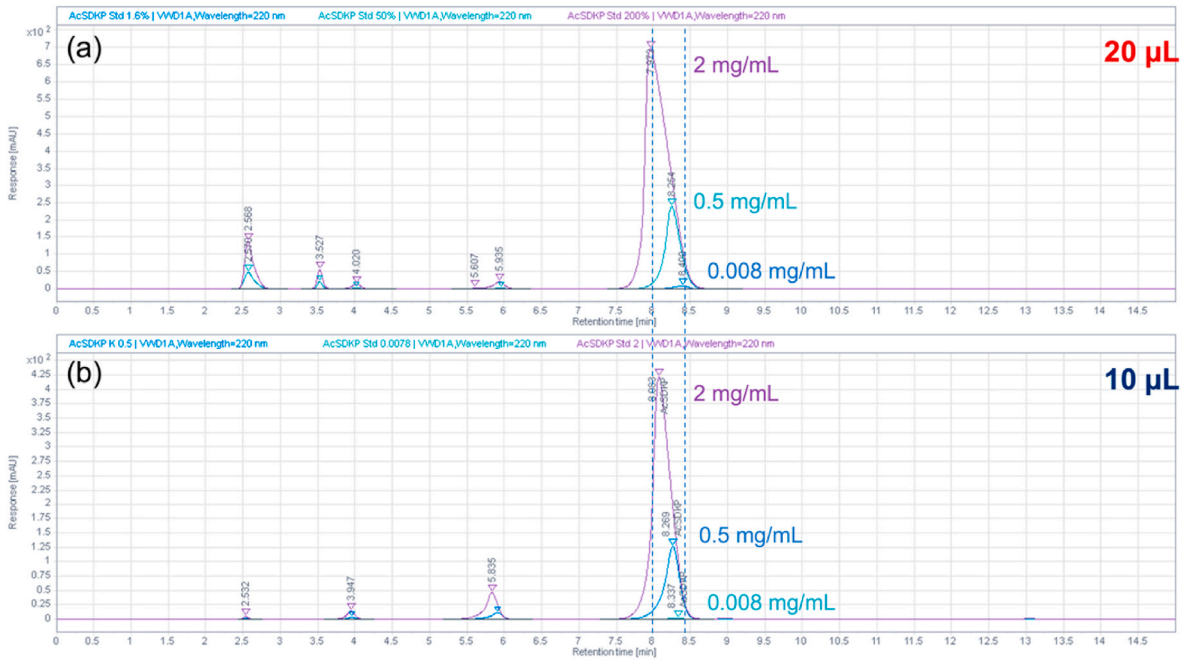

Fig. 7. Chromatograms of three calibration standard solutions in the calibration curve ranged from 8 µg/mL, 0.5 and 2 mg/mL at two different injection volumes of (a) 20 µl and (b) 10 µL; mobile phase flow rate 1 mL/min; a linear gradient (ACN: 3%–9.7% (v/v) in 15 min); VWD detector wavelength 220 nm; column temperature 25 °C. The figure showed that the peak shifts were attenuated, and all the peaks were within the 2.5% window after halving the injection volume to 10 µL. Variations in retention times between runs are expected, thus 2.5% was set as the acceptable window in this method due to the robustness of the method and Quality by Design.

$$\begin{aligned} Theoretical\ plate = {} & 12125.0877 + 1339.4269 \times \%B_i - 1626.7860 \times \%B_s \\ & - 5387.884586 \times FR - 599.5389 \times pH - 168.7069 \times T + 3.0456 \times T^2 \\ & - 107.6290 \times \%B_i \times \%B_s - 424.0912 \times \%B_i \times FR - 3.3746 \times \%B_i \times T \\ & + 1479.9857 \times \%B_s \times FR \end{aligned} \tag{11}$$

3.1.3. Multiple response optimisation

The optimal fabricating condition was determined by multiple response optimisation (MRO) as shown in Fig. 6, aiming to achieve the largest capacity factor, resolution and theoretical plate, and the lowest tailing factor. The optimal running condition for Ac-SDKP utilises phosphate buffer at pH 2.5 and acetonitrile as mobile phases, which starts at 3% (v/v) acetonitrile and increases to 9.7% (v/v) over 15 min at a flow rate of 1 mL/min. The injection volume was initially fixed at 20 µL, to maximise the ranges of detection and quantitation. The predicted capacity factor, resolution, tailing factor and theoretical plate running at the optimal chromatographic condition were 2.400, 5.779, 1.22, and 5778 respectively while the experimental results were 2.138, 5.970, 1.15, and 5680 respectively. The measured values were −10.9%, 3.3%, −5.7%, and −1.7% different from the predicted values for capacity factor, resolution, tailing factor, and theoretical plate respectively. Although there were discrepancies between the measured and predicted values for all responses, the results still demonstrated that these models had sufficient predictive ability.

However, mass overloading was observed in the column using the injection volume of 20 µL, with the peak fronting observed. The peak shifts exceeded the relative retention time window of 2.5%, at the lower concentrations of the calibration curve with the red arrow pointed in Fig. 7 (a). This was likely to be due to the repulsion between the cationic peptide on the stationary phase and preventing the occupancy of the high-energy sites in the deeper C18 layer by the solute [37], as the peptide remains cationic at pH 2.5. Moreover, the broad and asymmetrical peak observed in the chromatogram could also be explained by the slow sorption-desorption kinetics on the silanols of the stationary phase [38]. Therefore, the injection volume was finally reduced to 10 µL, to further minimise the shifting of the retention time. The retention time shift was still present with the injection volume of 10 µL, but the shift was much attenuated and maintained within 2.5% of variation as shown in Fig. 7 (b). It was noted that the reduction of the injection volume had impacts on the ATP, mainly reducing the tailing factor, as the peak area was reduced and there was less mass overloading on the column. Moreover, it also impacted the capacity factor slightly, attenuating the shift of the peak retention time. Despite these impacts on the ATP, it was vital to reduce the mass overloading on the column, avoiding the diminishments of the efficiency and the assay sensitivity. Hence, the injection volume was adjusted after the DOE optimisation, as a mitigation to the mass overloading.

3.2. Method validation

3.2.1. Specificity

The specificity of the method was evaluated by comparing the chromatograms of the peptide in water, PBS, CSNG, DMEM complete media, FluoroBrite complete media and HBSS with their respective blank solutions. Thus, 10 µL of these solutions were injected into the HPLC system individually, and the chromatograms are shown in Fig. 8. In the chromatograms for the samples containing the peptide, as present in Fig. 8 (a)–(f), the analyte was eluted as a single peak and well separated from other peaks presented. No co-eluting peak at the retention time of the peptide was observed, which indicated that the analyte peak was pure, and the method was specific. However, the AUC of the peak corresponding to the peptide was significantly larger with PBS spiked samples, while the AUC was lower with FluoroBrite spiked samples, which indicated the likelihood of matrix effects. In Fig. 8 (g)–(l), no peak of analyte was present for the blank PBS, water and HBSS solutions, while no peak with a retention time of 8.5 min was observed despite the presence of other peaks in the chromatogram, which also elucidated that the other components in the sample did not interfere with the peak of the analyte. The presence of other peaks in Fig. 8 (h), (j) and (k) likely corresponded to the presence of other components in the solutions that are not removed by diafiltration. The peaks at 3.9 and 6.5 min observed

Fig. 8. Chromatograms of the peptide standard in (a) water, (b) chitosan-TPP nanogel filtrate, (c) PBS, (d) DMEM complete media, (e) FluoroBrite complete media, (f) HBSS. The concentration of peptide was 1.0 mg/mL in all spiked samples. Figure (g–l) shows the respective blank solutions.

Table 2
System suitability results of the proposed HPLC method on two different HPLC systems.

System suitability parameters	Acceptable criterion	HLPC 1	HPLC 2
Retention time	RSD ≤1%	0.1%	0.5%
Peak area	RSD ≤1%	0.2%	0.8%
Capacity factor (k)	k ≥ 2.0	2.237	2.256
Resolution (Rs)	Rs ≥ 2.0	6.881	6.409
Tailing factor (T)	T ≤ 1.5	0.90	0.93
Theoretical plates (N)	N ≥ 2000	7349	7283

in Fig. 8(a–f) likely referred to the impurities present in the Ac-SDKP.

3.2.2. System suitability

A system suitability test was performed with a 1 mg/mL validation standard solution on two different HPLC systems. A total of 6 injections of the standard were injected into the column. The capacity factor, resolution, tailing factor, theoretical plates, and relative standard deviations (RSD) for retention time and peak area were determined and presented as the average in Table 2.

3.2.3. Linearity and range

The calibration curve was established with 13 concentrations as shown in Fig. S3, with the solution with the lowest concentration of 3.9 μg/mL being undetectable. Therefore, the range of the assay method is between 7.8 μg/mL to 2.0 mg/mL. The correlation coefficient of the calibration was 0.999, which was acceptable under the criterion. The result elucidated a good correlation between the peak area and the concentration within the range. The regression equation was $y = 3661x + 11.88$. The range established in this method was much higher compared to the reported LC-MS or EIA methods, where the range of these methods was between 0.5 and 100 ng/mL [11,13,15].

3.2.4. Limit of detection and limit of quantification

The LOD and LOQ were determined from equations (2) and (3), using the standard deviation of y-intercept in the calibration curve as σ. The LOD and LOQ were 1.0 and 2.9 μg/mL respectively.

3.2.5. Accuracy

Accuracy was reported as the recovery percentage of the known peptide added to five matrix solutions. The method involved spiking the PBS, CSNG, HBSS, DMEM and FluoroBrite complete media with Ac-SDKP in water at three different concentrations (0.75, 1.00 and 1.50 mg/mL), with the results shown in Table 3. The % recovery obtained in the spiking of the sample with PBS was higher than in other matrices and in water. The CSNG is predominantly water and salt, as the Amicon ultra filter trapped all nanoparticles during the centrifugation, where both PBS and HBSS contained phosphate, sodium and potassium salts. HBSS also contained magnesium salts and glucose. As for the DMEM and FluoroBrite complete media, they are culture media for various in vitro cell studies, with the DMEM containing phenol red but not the latter. The complete culture media contained FBS, glucose, inorganic salts, various vitamins and amino acids. After diafiltration, molecules with a

Table 3
Results of accuracy tests for determination of peptide Ac-SDKP in phosphate buffer saline and matrix solution samples.

Spiked samples	Concentrations (mg/mL)	Purity (% Area)	Area	Percentage recovery		Criterion
			RSD, %	Average (%)	RSD, %	
PBS	0.75	96.6 ± 0.4	3.7%	82.2	3.7%	RSD <10%
	1.00	97.1 ± 0.0	0.3%	108.7	0.3%	
	1.50	97.8 ± 0.2	0.2%	161.0	0.2%	
Chitosan-TPP nanogels filtrate (CSNG)	0.75	86.5 ± 0.8	0.6%	73.8	0.6%	
	1.00	88.8 ± 0.2	0.5%	97.9	0.5%	
	1.50	90.5 ± 0.1	0.7%	151.6	0.7%	
DMEM complete media	0.75	59.4 ± 0.5	1.9%	78.2%	1.9%	
	1.00	65.9 ± 1.3	0.9%	105.5%	0.9%	
	1.50	82.7 ± 0.6	0.2%	159.7%	0.2%	
FluoroBrite complete media	0.75	64.2 ± 1.7	0.7%	73.1%	0.7%	
	1.00	75.8 ± 2.3	0.8%	97.0%	0.8%	
	1.50	85.8 ± 0.5	0.8%	144.3%	0.8%	
HBSS	0.75	90.5 ± 0.1	0.4%	74.4%	0.4%	
	1.00	89.8 ± 0.9	5.3%	100.7%	5.3%	
	1.50	90.5 ± 0.1	0.3%	153.9%	0.3%	

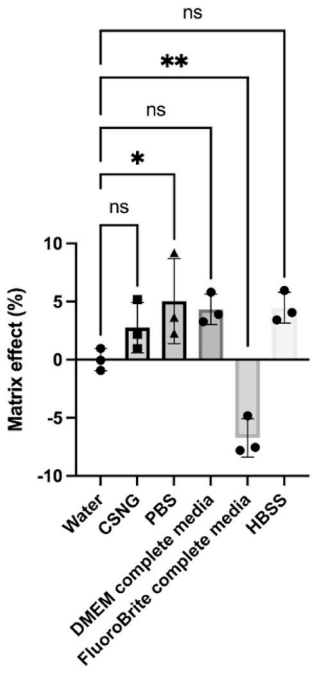

Fig. 9. Matrix effects of the CSNG, PBS, HBSS, DMEM and FluoroBrite complete media on the chromatographic method. Analysis of variance (ANOVA) was performed to determine the statistical significance of the effects for each matrix on the chromatographic method, as compared to the result in water. ns refers to p-value > 0.05, while * and ** refer to p-value < 0.05 and p-value <0.01 respectively.

size above 3000 Da, such as the proteins from FBS, were likely removed as the MWCO of the filter was 3000 Da.

The matrix effects of the DMEM complete media, FluoroBrite complete media, CSNG, PBS and HBSS were determined by equation (4), with the values of 7.0 ± 1.3%, −6.7 ± 1.7%, 2.6 ± 2.2%, 4.9 ± 3.8% and 4.3 ± 1.3% respectively. However, the matrix effects for DMEM complete media, CSNG, and HBSS were not statistically significantly different from water according to the ANOVA as shown in Fig. 9, and thus the matrix effects of these matrices are negligible. Interestingly, the presence of phenol red in DMEM complete media did not affect the peptide quantification method. Conversely, the matrix effects of FluoroBrite complete media and PBS demonstrated significant differences from water, where FluoroBrite complete media and PBS demonstrated negative and positive matrix effects respectively. Despite the relatively low purity of peptide used due to the cost, the purity of the peptide was measured at over 85% in all spiked samples with PBS, HBSS and CSNG solutions, which was close to the manufacturer's reported value of 90%. However, the purity dropped below 80% in spiked samples with the DMEM and FluoroBrite complete media, due to the presence of other components in the matrix solution that were not filtered by diafiltration, such as non-essential amino acids, vitamins, penicillin or streptomycin. Thus, the % area decreased when the complete media were used. The results showed that the method remains robust, albeit more complex matrix solutions were used. Moreover, the less pure peptide used in the study did not impact the method development and validation, as the % area would reflect the purity of the analytes tested.

3.2.6. *Precision – repeatability and intermediate precision*

The average, SD and RSD of the retention time, peak area, and height for the 10 replicates in repeatability measurement were presented in Table 4, with the experimental RSD for all parameters below 1% and fulfilling the criteria. The result elucidated that the method is precise and the intra-day variation on the instrument was minimal.

In contrast, the intermediate precision assessed the method's

Table 4
Intermediate precision and repeatability of the method.

Instrument	HPLC 1 (Agilent 1260)			HPLC 2 (Agilent 1200)			
Intermediate precision (n = 3)							
Concentrations (mg/mL)	0.5	1.0	1.5	0.5	1.0	1.5	Criterion
Operator 1 inter-day RSD	0.37%	0.26%	0.75%	0.93%	1.64%	0.69%	RSD <2%
Operator 2 inter-day RSD	1.32%	1.37%	1.32%	0.1%	0.46%	0.15%	RSD <2%
Instrument RSD	1.26%	1.04%	0.88%	0.16%	0.36%	0.11%	RSD <2%
Repeatability (n = 10)	**Average**	**RSD, %**					**Criterion**
Resolution	8.203	0.12%					RSD<1%
Area	3749.4	0.22%					RSD<1%
Height	242.09	0.92%					RSD<1%

Table 5
Deliberate variations in analytical conditions to determine the robustness of the HPLC-UV assay method. The varied factors were bolded and italicised.

Trial	Opt.	A	B	C	D	E	F	G	H
T (°C)	25	***20***	***30***	25	25	25	25	25	25
%Bs	3	3	3	***2***	***4***	3	3	3	3
%Bi	6.7	6.7	6.7	6.7	6.7	6.7	6.7	6.7	6.7
FR (mL/min)	1	1	1	1	1	***0.8***	***1.2***	1	1
pH	2.5	2.5	2.5	2.5	2.5	2.5	2.5	***2.4***	***2.6***
Predicted Rf	2.400	2.657	2.193	3.100	1.723	2.428	2.395	2.464	2.359
Experimental Rf	2.261 ± 0.001	2.479 ± 0.001	2.105 ± 0.003	3.042 ± 0.004	1.856 ± 0.001	2.955 ± 0.002	2.107 ± 0.007	2.312 ± 0.004	2.255 ± 0.002
% Difference	6.1%	7.2%	4.2%	1.9%	−7.1%	−17.8%	13.6%	6.6%	4.6%
Area	3687.6 ± 8.7	3688.5 ± 2.3	3696.7 ± 1.9	3702.8 ± 1.8	3696.7 ± 0.6	4607.4 ± 4.8	3731.6 ± 2.3	3703.2 ± 0.1	3762.5 ± 0.1
% Difference (vs Opt.)	N/A	0.0%	0.2%	0.4%	0.2%	24.9%	1.2%	0.4%	2.0%

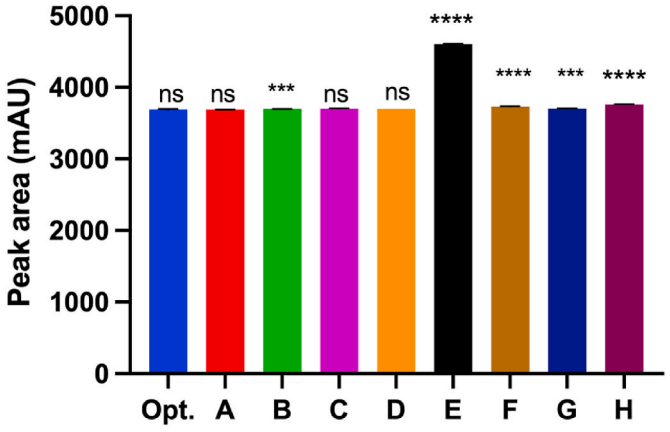

Fig. 10. Robustness of method in terms of peak area with the variations in temperature (A & B), starting %B (C & D), flow rate (E & F), and pH (G & H). One-way ANOVA was performed to determine if the variations result in a significant difference in the retention time and peak area. Dunnett's test was performed to compare all variations to the standard method. *** p-value < 0.001, **** p-value < 0.0001 and ns denoted not significant. Each data point is presented as average, while the error bar refers to the standard deviation, which might be too small to be observed in the figure.

resistance to different instrumentation, time of analysis, and analyst to the initial method developed. The RSD for the inter-day precisions for both analysts 1 and 2 and on both Agilent Infinity 1260 and 1200 HPLC systems were lower than the limit of 2%, which indicated that the method was resistant to variations in the analyst and time. The instrumental RSD, which included all runs on that instrument regardless of the day and analyst, was also smaller than the criterion and thus demonstrated that the method was precise and repeatable in different instrumental systems.

3.2.7. Robustness

The robustness of the method was evaluated by deliberate alterations of the temperature, $\%B_s$, $\%B_i$, flow rate, and pH, as shown in Table 5. For the capacity factor of the analyte peak, they are first predicted based on the correlations established in the method operable design space and subsequently compared with the experimental result. The percentage difference between the predicted and experimental results was less than 7.5% for most of the alterations, which were set as the acceptance criteria. However, changing the flow rate had a notable impact on the capacity factor of the peak of an analyte, exceeding the 10% difference between the predicted and experimental results. The result indicated that controlling the flow rate (ie. Linear velocity) is critical to avoid any impact on the ATP. Temperature, $\%B_s$, and pH were found to impact the capacity factor of the analyte peak, but their effects could largely be modelled by the correlation established. Altering the temperature resulted in shifts of the retention as the temperature impacts the analyte diffusivity, viscosity [39], dielectric constant [40], and surface tension of the mobile phase, where the analyte diffusivity improved and the rest of the factors decreased under the elevated temperature, resulting in the decrease of the solute elution. Nevertheless, modifying $\%B_s$ does not affect the interaction between the analyte and the stationary phase, as $\%B_s$ refers to the starting % of the organic solvent in the mobile phase. Thus, with the same eluting gradient, the retention time changes with the $\%B_s$ inversely and linearly. The pH of the buffer is another factor crucial to determining the ionization of the peptide, where the pH of the buffer was close to the isoelectric point of the peptide. Therefore, any change in the pH of the buffer would affect the ionization of the peptide and subsequently the capacity factor.

Regarding the peak area, as it is not an ATP defined above, the percentage difference was calculated between the results obtained in the optimal condition and altered conditions. ANOVA was performed to determine whether the differences between the peak area obtained from these conditions were significant, as shown in Fig. 10. The acceptable criteria were set as a percentage difference of 2% between the peak area obtained from the optimal and altered conditions. The result indicated that the differences were significant, especially when $\%B_s$ was increased by 1%, and when flow rate and buffer pH were changed. The peak area measured in these conditions was larger as compared to the original method. However, the degree of differences was small, with less than 2% for most of the other alterations, revealing the robustness of the model. Similarly, decreasing the flow rate by 10% significantly increased the peak area of the analyte peak by approximately 25%, which demonstrated the importance of controlling the flow rate in the method. The reduction in flow rate also indicated a slower velocity through the detection flow cell, of which each molecule contributed more to the measured absorbance at the set detector sensitivity (0.1 AUFS) [41]. Noteworthy, the flow rate at 0.8 mL/min was not in the method operable design region, as the latter was between 1.0 and 1.5 mL/min. Thus, this discrepancy also revealed the significance of performing the method within the MODR, and any extrapolation outside the MODR was not feasible. Increasing the flow rate to 1.2 mL/min, which was in the MODR, altered the peak area to a much lesser degree, with only a 1.2% difference from that of optimal condition. Furthermore, increasing the pH to 2.6 also impacted the peak area, but the percentage difference calculated was 2.0%. The increase was likely due to more interactions between the solute and stationary phase when the pH of the buffer increased. Moreover, pH 2.6 is closer to the isoelectric point of the peptide (estimated to be pH 3), where more peptides were neutral in charge and interacted more strongly with the stationary phase. Conversely, the peak area measured with pH 2.4 buffer was significantly different from the proposed method, but the percentage difference was much smaller. The result demonstrated that pH 2.6 is likely the cut off pH for the method without altering the accuracy. All in all, the results indicated that the method is robust within the MODR.

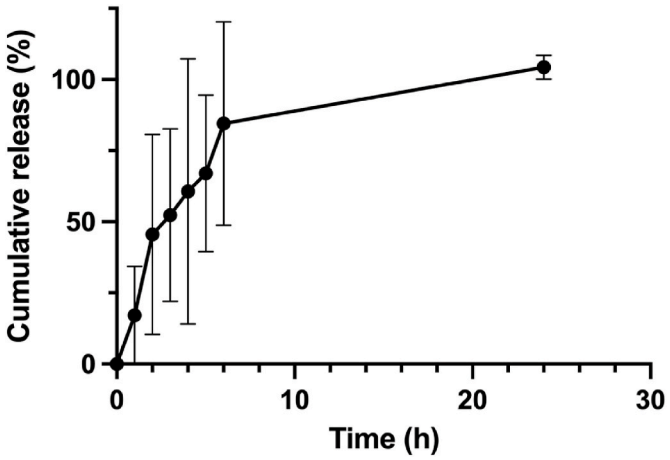

Fig. 11. Cumulative release of Ac-SDKP from the chitosan-TPP nanogels over 24 h.

3.3. Determining the encapsulation efficiency and drug release of Ac-SDKP from chitosan-TPP nanogels

The encapsulation efficiency of Ac-SDKP in the chitosan-TPP nanogels was determined as 36.0 ± 10.8%. The drug release profile of Ac-SDKP from the nanogels was shown in Fig. 11, where a rapid release of the peptide over the first 6 h. The cumulative release of Ac-SDKP measured at 24 h was close to 100%. The results demonstrated the method was suitable for quantifying the peptide from the nanogels at concentrations commensurate with therapeutic doses and in phosphate buffer.

4. Conclusion

A simple, novel and accurate HPLC-UV method for quantification of antifibrotic peptide N-acetyl-seryl-aspartyl-lysyl proline (Ac-SDKP) has been developed and validated in this study using an analytical quality by design approach. The method was optimised via the Design of Experiment to identify the optimal chromatographic condition, where the obtained capacity factor, resolution, tailing factor, and theoretical plate counts fulfilled the ICH guidelines. The validated chromatography condition utilises phosphate buffer at pH 2.5 and acetonitrile as mobile phases, which starts at 3% (v/v) acetonitrile and increases to 9.7% (v/v) over 15 min at a flow rate of 1.0 mL/min at 25 °C. The injection volume is set at 10 μL and the VWD detector wavelength is 220 nm. The new analytical method described is advantageous as it utilises standard HPLC settings and does not involve the use of expensive equipment or procedures, such as LC-MS/MS or ELISA. We believe the method is particularly well-suited to pharmaceutical research and the development of dosage forms for peptides as it is capable of detecting peptides at high concentrations covering the range for the experimental therapeutic doses, especially in PBS for in vitro drug release study. Moreover, the peptide concentration in a chitosan-TPP nanogels formulation was also successfully determined, demonstrating the applicability of the method. Other more complex matrix solutions, including HBSS, DMEM and FluoroBrite complete media, were also tested with the chromatographic method, demonstrating the robustness of the method.

Declaration of competing interest

No conflict of interest.

Acknowledgement

This work was also supported by the EPSRC Centre in Doctoral Training for Nanomedicine and Advanced therapeutics [EP\L01646X] awarded to HMKH. The authors would like to express their appreciation for the continuous and kind support from the funder EPSRC.

Appendix A. Supplementary data

Supplementary data to this article can be found online at https://doi.org/10.1016/j.ab.2022.114793.

References

[1] S. Rasoul, O.A. Carretero, H. Peng, M.A. Cavasin, J. Zhuo, A. Sanchez-Mendoza, D. R. Brigstock, N.E. Rhaleb, Antifibrotic effect of Ac-SDKP and angiotensin-converting enzyme inhibition in hypertension, J. Hypertens. 22 (2004) 593–603, https://doi.org/10.1097/00004872-200403000-00023.

[2] A.T. Mnguni, M.E. Engel, M.S. Borkum, B.M. Mayosi, The Effects of Angiotensin Converting Enzyme Inhibitors (ACE-I) on human nacetyl- seryl-aspartyl-lysyl-proline (Ac-SDKP) Levels: a systematic review and meta- analysis, PLoS One 10 (2015), e0143338, https://doi.org/10.1371/journal.pone.0143338.

[3] N. Kumar, C. Yin, The anti-inflammatory peptide Ac-SDKP: synthesis, role in ACE inhibition, and its therapeutic potential in hypertension and cardiovascular diseases, Pharmacol. Res. 134 (2018) 268–279, https://doi.org/10.1016/j.phrs.2018.07.006.

[4] Y. Zuo, B. Chun, S.A. Potthoff, N. Kazi, T.J. Brolin, D. Orhan, H.C. Yang, L.J. Ma, V. Kon, T. Myöhänen, N.E. Rhaleb, O.A. Carretero, A.B. Fogo, Thymosin β4 and its degradation product, Ac-SDKP, are novel reparative factors in renal fibrosis, Kidney Int. 84 (2013) 1166–1175, https://doi.org/10.1038/ki.2013.209.

[5] J. Sanchez-Mas, A. Lax, M.C. Asensio-Lopez, M.J. Fernandez-Del Palacio, L. Caballero, I.P. Garrido, F. Pastor, J.L. Januzzi, D.A. Pascual-Figal, Galectin-3 expression in cardiac remodeling after myocardial infarction, Int. J. Cardiol. 172 (2014) e98–e101, https://doi.org/10.1016/j.ijcard.2013.12.129.

[6] H. Peng, O.A. Carretero, D.R. Brigstock, N. Oja-Tebbe, N.E. Rhaleb, Ac-SDKP reverses cardiac fibrosis in rats with renovascular hypertension, Hypertension 42 (2003) 1164–1170, https://doi.org/10.1161/01.HYP.0000100423.24330.96.

[7] E. Conte, E. Fagone, E. Gili, M. Fruciano, M. Iemmolo, M.P. Pistorio, D. Impellizzeri, M. Cordaro, S. Cuzzocrea, C. Vancheri, Preventive and therapeutic effects of thymosin β4 N-terminal fragment Ac-SDKP in the bleomycin model of pulmonary fibrosis, Oncotarget 7 (2016) 33841–33854, https://doi.org/10.18632/oncotarget.8409.

[8] P. Nakagawa, C.A. Romero, X. Jiang, M.D. Ambrosio, G. Bordcoch, E.L. Peterson, P. Harding, X.P. Yang, O.A. Carretero, Ac-SDKP decreases mortality and cardiac rupture after acute myocardial infarction, PLoS One 13 (2018), e0190300, https://doi.org/10.1371/journal.pone.0190300.

[9] L. Zhu, X.P. Yang, B. Janic, N.E. Rhaleb, P. Harding, P. Nakagawa, E.L. Peterson, O. A. Carretero, Ac-SDKP suppresses TNF-α-induced ICAM-1 expression in endothelial cells via inhibition of ικB kinase and NF-κB activation, Am. J. Physiol. Heart Circ. Physiol. 310 (2016) H1176–H1183, https://doi.org/10.1152/ajpheart.00252.2015.

[10] M. Song, H. Jang, J. Lee, J.H. Kim, S.H. Kim, K. Sun, Y. Park, Regeneration of chronic myocardial infarction by injectable hydrogels containing stem cell homing factor SDF-1 and angiogenic peptide Ac-SDKP, Biomaterials 35 (2014) 2436–2445, https://doi.org/10.1016/j.biomaterials.2013.12.011.

[11] C. Junot, F. Theodoro, J. Thierry, G. Clement, J. Wdzieczak-Bakala, E. Ezan, Development of an enzyme immunoassay for a stable amidated analog of the hemoregulatory peptide Acetyl-Ser-Asp-Lys-Pro, J. Immunoassay Immunochem. 22 (2001) 15–31, https://doi.org/10.1081/IAS-100102895.

[12] P. Pradelles, Y. Frobert, C. Créminon, E. Liozon, A. Massé, E. Frindel, Negative regulator of pluripotent hematopoietic stem cell proliferation in human white blood cells and plasma as analysed by enzyme immunoassay, Biochem. Biophys. Res. Commun. 170 (1990) 986–993, https://doi.org/10.1016/0006-291X(90)90489-A.

[13] K. Inoue, A. Ikemura, Y. Tsuruta, K. Tsutsumiuchi, T. Hino, H. Oka, On-line solid-phase extraction LC-MS/MS for the determination of Ac-SDKP peptide in human plasma from hemodialysis patients, Biomed. Chromatogr. 26 (2012) 137–141, https://doi.org/10.1002/bmc.1636.

[14] C. Mesmin, S. Cholet, A. Blanchard, Y. Chambon, M. Azizi, E. Ezan, Mass spectrometric quantification of AcSDKP-NH 2 in human plasma and urine and comparison with an immunoassay, Rapid Commun. Mass Spectrom. 26 (2012) 163–172, https://doi.org/10.1002/rcm.5326.

[15] K. Inoue, A. Ikemura, Y. Tsuruta, K. Watanabe, K. Tsutsumiuchi, T. Hino, H. Oka, Quantification of N-acetyl-seryl-aspartyl-lysyl-proline in hemodialysis patients administered angiotensin-converting enzyme inhibitors by stable isotope dilution liquid chromatography-tandem mass spectrometry, J. Pharm. Biomed. Anal. 54 (2011) 765–771, https://doi.org/10.1016/j.jpba.2010.10.009.

[16] C. Junot, A. Pruvost, C. Créminon, J.M. Grognet, H. Benech, E. Ezan, Characterization of immunoreactive acetyl-Ser-Asp-Lys-Pro in human plasma and urine by liquid chromatography-electrospray mass spectrometry, J. Chromatogr. B Biomed. Sci. Appl. 752 (2001) 69–75, https://doi.org/10.1016/S0378-4347(00)00520-X.

[17] U. Sharma, N.E. Rhaleb, S. Pokharel, P. Harding, S. Rasoul, H. Peng, O. A. Carretero, Novel anti-inflammatory mechanisms of N-Acetyl-Ser-Asp-Lys-Pro in hypertension-induced target organ damage, Am. J. Physiol. Heart Circ. Physiol. 294 (2008) H1226–H1232, https://doi.org/10.1152/ajpheart.00305.2007.

[18] H. Singh, L.K. Khurana, R. Singh, Pharmaceutical development, Pharm. Med. Transl. Clin. Res. (2017) 33–46, https://doi.org/10.1016/B978-0-12-802103-3.00003-1.
[19] D. Elder, A. Teasdale, ICH Q9 Quality Risk Management, ICH Qual. Guidel., 2017, pp. 579–610, https://doi.org/10.1002/9781118971147.ch21.
[20] J. Pogány, ICH pharmaceutical quality system Q10, WHO Drug Inf. 22 (2008) 177–181.
[21] N.V.V.S.S. Raman, U.R. Mallu, H.R. Bapatu, Analytical quality by design approach to test method development and validation in drug substance manufacturing, J. Chem. 2015 (2015) 1–8, https://doi.org/10.1155/2015/435129, 435129.
[22] R. Peraman, K. Bhadraya, Y. Padmanabha Reddy, Analytical quality by design: a tool for regulatory flexibility and robust analytics, Int. J. Anal. Chem. (2015), https://doi.org/10.1155/2015/868727, 2015.
[23] D.K. Lloyd, J. Bergum, Application of quality by design (QbD) to the development and validation of analytical methods, Specif. Drug Subst. Prod. Dev. Valid. Anal. Methods. 405 (2013) 29–72, https://doi.org/10.1016/B978-0-08-098350-9.00003-5.
[24] H. Bhutani, M. Kurmi, S. Singh, S. Beg, B. Singh, Quality by design (QbD) in analytical sciences: an overview, Pharmatimes 46 (2014) 71–75.
[25] K.Y. Patel, Z.R. Dedania, R.R. Dedania, U. Patel, QbD approach to HPLC method development and validation of ceftriaxone sodium, Futur. J. Pharm. Sci. 7 (2021) 1–10, https://doi.org/10.1186/s43094-021-00286-4.
[26] M.V. Krishna, R.N. Dash, B. Jalachandra Reddy, P. Venugopal, P. Sandeep, G. Madhavi, Quality by Design (QbD) approach to develop HPLC method for eberconazole nitrate: application oxidative and photolytic degradation kinetics, J. Saudi Chem. Soc. 20 (2016) S313–S322, https://doi.org/10.1016/j.jscs.2012.12.001.
[27] U.S. Food & Drug Administration, QbD Considerations for Analytical Methods - FDA Perspective, IFPAC Annu. Meet., 2013.
[28] E.C. Harrington, The desirability function, Ind. Qual. Control. 21 (1965) 494–498.
[29] G. Derringer, R. Suich, Simultaneous optimization of several response variables, J. Qual. Technol. 12 (1980) 214–219, https://doi.org/10.1080/00224065.1980.11980968.
[30] E.M. Agency, Validation of analytical procedures: text and methodology, Prescrire Int. 20 (2011) 278.
[31] G.A. Shabir, Step-by-step analytical methods validation and protocol in the quality system compliance industry, J. Valid, Technol. 10 (2005) 314–325.
[32] H. Naseef, R. Moqadi, M. Qurt, Development and validation of an HPLC method for determination of antidiabetic drug alogliptin benzoate in bulk and tablets, J. Anal. Methods Chem. (2018), https://doi.org/10.1155/2018/1902510, 2018.
[33] H.M.K. Ho, D.Q.M. Craig, R.M. Day, Design of experiment approach to modeling the effects of formulation and drug loading on the structure and properties of therapeutic nanogels, Mol. Pharm. 19 (2022) 602–615, https://doi.org/10.1021/acs.molpharmaceut.1c00699.
[34] A.D. McNaught, A. Wilkinson, Compendium of Chemical Terminology, Blackwell Science Oxford, 2014. http://goldbook.iupac.org/PDF/goldbook.pdf%5Cnhttp://goldbook.iupac.org/I03352.html.
[35] J.W. Dolan, Flow-rate and peak spacing, LC-GC, Eure 16 (2003) 252–255.
[36] H.G. Barth, Chromatography Fundamentals, Part V: Theoretical Plates: Significance, Properties, and Uses, 2018.
[37] C. Wang, Z. Guo, Z. Long, X. Zhang, X. Liang, Overloading study of basic compounds with a positively charged C18 column in liquid chromatography, J. Chromatogr. A 1281 (2013) 60–66, https://doi.org/10.1016/j.chroma.2013.01.074.
[38] E. Peris-García, M.C. García-Alvarez-Coque, S. Carda-Broch, M.J. Ruiz-Angel, Effect of buffer nature and concentration on the chromatographic performance of basic compounds in the absence and presence of 1-hexyl-3-methylimidazolium chloride, J. Chromatogr. A 1602 (2019) 397–408, https://doi.org/10.1016/j.chroma.2019.06.061.
[39] T. Greibrokk, T. Andersen, High-temperature liquid chromatography, J. Chromatogr. A 1000 (2003) 743–755.
[40] B.W. Wenclawiak, S. Giegold, T. Teutenberg, High-temperature liquid chromatography, Anal. Lett. 41 (2008) 1097–1105.
[41] D.R. Stoll, Effect of flow rate on UV detection in liquid chromatography, LCGC North Am. 37 (2019) 846–850. https://www.chromatographyonline.com/view/effects-flow-rate-uv-detection-liquid-chromatography-0.